Hindawi
Advances in Civil Engineering
Volume 2022, Article ID 5091895, 13 pages
https://doi.org/10.1155/2022/5091895

Research Article

Estimation of Hydraulic Properties in Permeable Pavement Subjected to Clogging Simulation

Guoyang Lu,[1] **Zijian He**,[1] **Pengfei Liu**,[2] **Zhihao He**,[2] **Gaoyang Li**,[1] **Hao Jiang**,[3] **and Markus Oeser**[2]

[1]*Department of Civil and Environmental Engineering, The Hong Kong Polytechnic University, Hong Kong, China*
[2]*Institute of Highway Engineering, RWTH Aachen University, Aachen 52074, Germany*
[3]*Chinese National Engineering Research Centre for Steel Construction (Hong Kong Branch), Z106, Z Block, Phase 8, The Hong Kong Polytechnic University, Hong Kong, China*

Correspondence should be addressed to Pengfei Liu; liu@isac.rwth-aachen.de

Received 29 July 2021; Revised 13 December 2021; Accepted 8 January 2022; Published 21 January 2022

Academic Editor: Ankit Gupta

Permeable pavements are often affected by pore clogging, which leads to their functional failure and reduced service life. However, the clogging mechanism and its impact on the permeability and complex pore microstructures in pervious pavement remain unclear. The aim of current study is to quantify the clogging behavior in pervious pavement materials and carry out investigations on the development of pore characteristics and permeability. Novel polyurethane-bound pervious mixture (PUPM) was adopted for comparative study in present research with conventional Porous Asphalt (PA). The Aachen Polishing Machine (APM) was selected to perfectly serve as a simulator for clogging process of pavement in the actual service condition. The permeability and pore microstructure of the pervious pavement material were then characterized by using the self-developed permeameter and X-ray Computed Tomography (CT) scanning, respectively. The development of pore characteristics in terms of clogging was experimentally illustrated. Based on the pore characteristics, the flow behavior of PUPM subjected to different clogging periods was predicted based on the developed non-Darcy flow model. The developed experiments and analysis can further strengthen the understanding of the clogging mechanism within the porous pavement material. The results can also serve for the optimization of the pervious pavement design in the engineering application.

1. Introduction

Permeable pavement is a type of pavement that allows rainwater and runoff to directly infiltrate into the pavement, rather than accumulating on the pavement surface. During the infiltration process, permeable pavement can also filter pollutants and particle matters from the water. So, the groundwater volume is not only replenished but the water quality can be also improved [1–3].

Permeable pavement systems exhibit water treatment potential and can retain up to 90% of particulate matter (PM) and total suspended solids (TSS), 65% of total phosphorus (TP), and 80% of total nitrogen (TN) [4, 5]. However, on the other hand, these particles that are present in the surface runoff can remain in the pores during the infiltration process. This buildup causes clogging in the pores, thereby gradually but significantly changing the hydraulic properties of the permeable pavement, which in turn will affect the mechanical performance of pavement [6–9]. Based on the previous research, clogging can be mainly due to two types of siltation processes: (a) long-term clogging process by urban runoff with fine particles and (b) short-term clogging by a sudden slump or landslide [10]. As the long-term service performance is greatly hindered by these clogging characteristics, studies have been conducted by applying fine particles accumulating in the void spaces of porous pavements based on different watering methods [11]. Clogging is found to be highly correlated with the particle size and volume, the flow rate, and pore characteristics of the pavement [12].

Previous research has been primarily focused on the observation of field measurement and macroscopic laboratory experiments. The microscopic characterization of the clogging such as the development of pore characteristics, particle distribution, and kinematics are still not clarified. A systematic understanding of the development of hydraulic and clogging mechanisms within the permeable pavement should be further established. Additionally, because most of the existing clogging experiments are based on modified permeameter by only changing the flow conditions, none of them can effectively simulate the clogging by considering the tires-road interaction.

In the present study, the objective is to quantify the clogging behavior in the permeable pavement materials (PPM) and the investigations on the development of pore characteristics and permeability taking into consideration the clogging effect. Thus, a more comprehensive understanding of the hydraulic properties of the PPM can be achieved. With the help of the derived non-Darcy flow equations in the previous study [13], the hydraulic properties of PPM during the clogging periods can be estimated. This could be a guideline for the accurate evaluation of the hydraulic properties of the PPM for future studies and practical application.

2. Materials and Methods

2.1. Materials. The porous pavement can achieve a high permeability performance because of its void-rich structure. However, the combination of this open-graded aggregate distribution design and the low shear force resistance binder, such as bitumen, results in weaknesses in durability and adhesion failure in the porous pavement. For this reason, a polyurethane-bound pervious mixture (PUPM) was developed by using the polyurethane (PU) to replace bitumen as the binder. Numerous researches have verified that PUPM has the notable mechanical and functional performance to be realized [14–17]. Moreover, during construction, PU can be cured at room temperature. Hence, a significant environmental benefit can be also achieved when compared to the conventional heating construction method of asphalt [18].

2.1.1. Mix Design. To investigate the pore characteristics of the PUPM, three types of the PUPM with different porosities were produced in this study: PUPM 8-H, PUPM 8, and PUPM 8-L, which denote mixture with maximum aggregate size 8 mm and high, normal, and low porosity levels, respectively. Conventional PPM, Porous Asphalt, PA 8, was also selected as the reference material to evaluate the properties of PUPM in this study, which is one of standard permeable pavement materials (RSto12, Guidelines for the Standardisation of Pavement Structures of Traffic Areas, edition 2012). The grain size distribution of all four chosen samples which were used in this study is illustrated in Figure 1.

2.1.2. Preparation of the PUPM Specimen. Figure 2 shows the manufacturing process of PUPM. The two components of the polyurethane (polymerize polyol and isocyanate) were mixed firstly to activate polymerization reaction. Once the binder

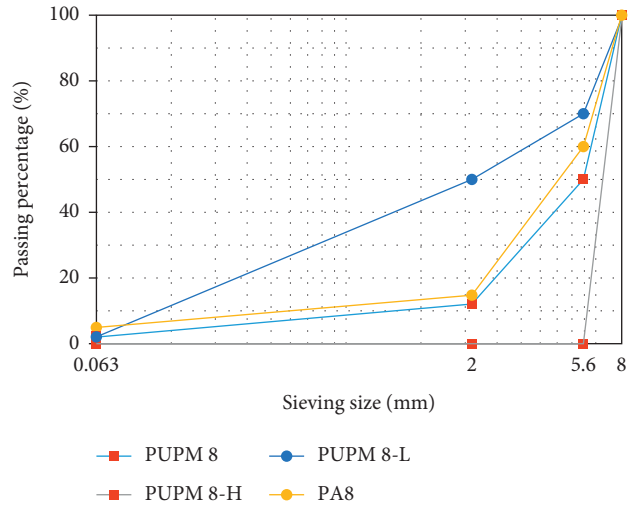

Figure 1: Grain size distribution of PUPM 8-H, PUPM 8, PUPM 8-L and PA 8.

was fully polymerized, they were mixed with aggregate. After all the aggregates can be observed evenly coated with polyurethane, the mixture was put into a mold with a length and width of 320 mm and 260 mm and a height of 40 mm for compaction. After a curing time of around 24 hours, 100 mm diameter cores were drilled. They were then weighted and used in the clogging simulation. The whole procedure of the specimen mixture was conducted at room temperature.

2.2. Laboratory Tests. To investigate the influence of the clogging behavior on the hydraulic properties of the specimens, several experimental procedures were designed. The first step was the simulation of clogging behavior in the specimens. The second step was to determine the clogging concentration of the influent and effluent. The third step was to evaluate the permeability of the specimens by conducting the permeability tests, and lastly, the pore characteristics of the specimens based on XCT were to be evaluated.

2.2.1. Clogging Simulation. To simulate the clogging in the laboratory, a simulation based on the Aachen Polishing Machine (APM) was carried out, as shown in Figure 3. By the aid of the APM, pavement samples can be exposed to a real tire loading (Type: Vanco 8, 165/75 R14 C 8PR 97/95RTL from Continental with shore hardness between 72 and 75 in level A). The main components of the APM are two independently working tires and a framework that can move forward and back. The sample is anchored to the track, and the wheels drive back and forward to simulate the condition on the pavement when a vehicle passes by. Since the pressure of the wheels in the APM system can be adjusted, the instrument can imitate all kinds of vehicle loads. For the clogging simulation in this study, sand, which has a grain size of up to 2 mm, was chosen as the clogging material. During the simulation, two different specimens were anchored to the track. Then, 40 grams of sand was sprinkled on the surface of the specimen. The vehicle tire in the APM then

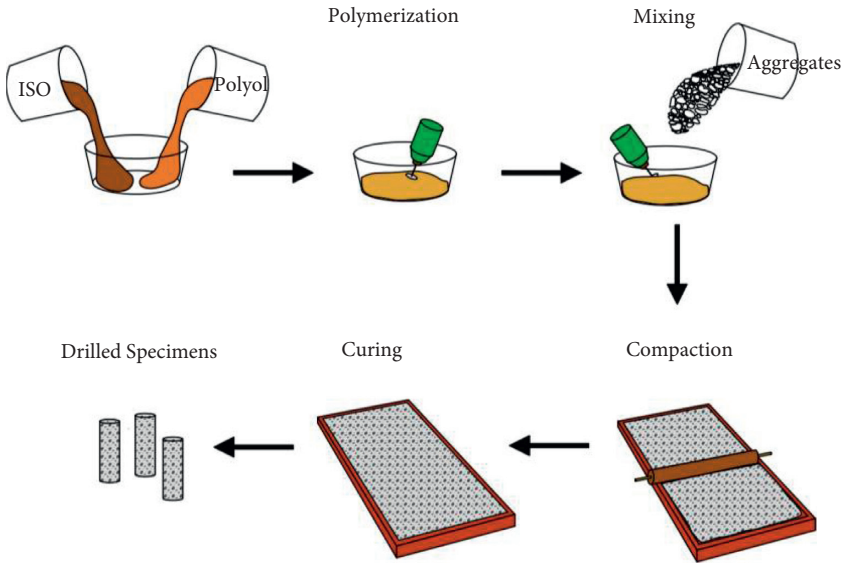

Figure 2: Manufacturing process of the PUPM specimens.

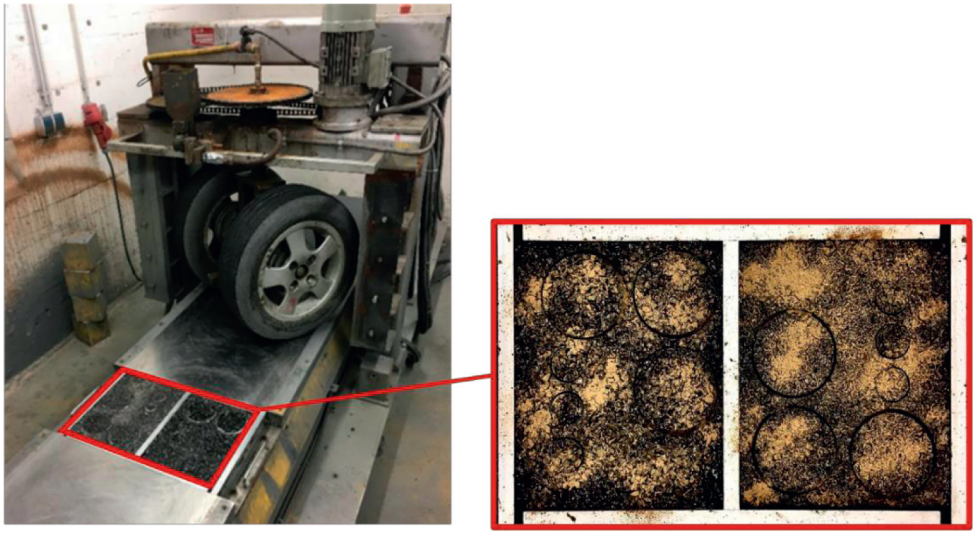

Figure 3: Clogging simulated by Aachen Polishing Machine (APM).

moved back and forth along the sample. The sled moved horizontally 9 times back and forth per minute, while the tires spun 41 rotations per minute. During the whole polishing process, water was sprinkled on the surface of the specimens. In this way, the sand would enter the void of the sample with the water and the pressure of the tire. All variants of the specimen (PUPM 8, PUPM 8-H, PUPM 8-L, and PA 8) were conducted with simulation. Each sample was processed for four different clogging periods: 20 minutes, 40 minutes, 60 minutes, and 80 minutes. These samples were then applied to the permeability tests. More information can be found in [19].

2.2.2. Clogging Concentration at Influent and Effluent. To investigate the clogging behaviors in the specimens, the clogging concentration at the influent and effluent from each specimen was tested. This can be described by two parameters: the strained clogging amount mass in the specimens and the particle mass separation efficiency.

The clogging period was set at 5 minutes. After the test started, the effluent flow through the test specimens as well as the overflow was collected in a pot. Every 5 minutes a new pot was replaced. The strained clogging agents from the collected effluents and overflow were dried and measured. In this way, the strained clogging mass during the clogging periods can be calculated by the subtraction of the clogging mass (in the effluent and overflow) from the influent. It can be illustrated from the following equation:

$$m_s = m_i - m_o - m_e, \tag{1}$$

where m_i, m_o, and m_e denote the dry clogging agents' mass in the influent, overflow, and effluent.

The particle mass separation efficiency η_m illustrates the percentage of the clogging amount throughout the specimen, and the equation is expressed as follows:

$$\eta_m(t) = \left(1 - \frac{[m_e](t)}{[m_i]}(t)\right) \times 100\%. \quad (2)$$

2.2.3. Permeability Test. Permeability describes the ability of a porous material to conduct water. The higher the permeability of a material, the faster the liquid can pass through. The permeability coefficient is a predictable indicator to represent the hydraulic characteristic of a material. In general, the permeability of the specimen can be described in horizontal and vertical directions. In this study, the vertical permeability of the specimens was investigated.

Based on the standard DIN EN 12697-19, a customized constant falling head permeameter, as in Figure 4 shown, is implemented for the test. More details can be referred to in the previous publication [19].

2.2.4. XCT Scanning. In order to quantify the pore characteristics of the specimens, a High-Resolution Computed Tomography and X-ray System (XCT) was used in this study. The X-ray system consists of a generator with 250-KV and a rotating scan table for the specimens. During the operation, the specimen was placed on the rotating scan table in the XCT system, then the X-ray generator of the XCT system shot a radiation beam to the specimen, and the reflected signal was received by the receptor and passed to the system for the analysis. In this study, all the scanning was accomplished by the XCT.

2.3. Models of Different Flow Behaviors

2.3.1. Flow Behavior with Low Velocity. The permeability of a porous media can be estimated not only by the experimental measurement but also by using empirical methods. Many researchers have attempted to estimate permeability with different models. One of the most recognized models was developed by Hazen; however, around one century later, Kozeny and Carman made a further step, which approached to delivering more accurate results [20].

The Kozeny–Carman model (KCM) is one of the well-known models that relates both permeability and porosity. It describes the relationship between the properties of the medium and the flow resistance in the pore channels. With the semiempirical-theoretical formula expressed in the following equation, the permeability of the porous media can be predicted [21].

$$K_{kcm} = \frac{\gamma_\omega}{\mu_\omega \cdot C_{k-c}} \cdot \frac{1}{S_{Ae}^2} \cdot \frac{{n_{eff}}^3}{\left(1 - n_{eff}\right)^2}, \quad (3)$$

where K_{kcm} is the Kozeny–Carman model permeability, γ_ω is the unit weight of water, μ_ω is the viscosity of water, C_{k-c} is the empirical Kozeny–Carman coefficient, S_{Ae} is the effective specific surface area, and n_{eff} is the effective porosity.

S_{Ae} can be obtained by the particle size distribution for the nonuniform spheres:

$$D_{\text{eff}} = \frac{100\%}{\sum\left(\phi_i / D_{li}^{0.5} \cdot D_{si}^{0.5}\right)}, \quad (4)$$

where D_{eff} is the effective diameter, φ_i is the percentage fraction of grain between the largest sieve size D_{li} and the smallest sieve size D_{si}.

Thus, the KCM model emphasizes grain size distribution (GSD) can be rewritten as follows:

$$K_{\text{KCM}}^{\text{GSD}} = \frac{\gamma_\omega}{\mu_\omega \cdot C_{k-c}} \cdot \left(\frac{100\%}{\sum\left(\phi_i / D_{li}^{0.5} \cdot D_{si}^{0.5}\right)}\right)^2 \cdot \frac{1}{S_{Ae}^2} \cdot \frac{{n_{\text{eff}}}^3}{\left(1 - n_{\text{eff}}\right)^2}. \quad (5)$$

Calculating with the conventional KCM can lead to a result with deviation because the equations parameters are dependent on uniform sphere particles and surrogate indices. Moreover, the aggregates of pavements are mostly irregular. Thus, a modified KCM is required for an appropriate prediction of permeable pavement. By considering the tortuosity τ, equation (3) can be rewritten as follows:

$$K_{KCM}^m = \frac{\gamma_\omega}{\mu_\omega \cdot C_{k-c}} \cdot \frac{n_{\text{eff}}}{\tau^2 S_{Ae}^2}. \quad (6)$$

2.3.2. Flow Behavior with High Velocity. Many researchers have used different methods to approach the characteristics of flow with high velocity. They can be classified into two groups: theoretical and empirical models. So, the empirical models in this study applied are from the Ergun and Ward, and the theoretical models are based on the capillaric models [13].

Based on the known information that the energy loss flow of the porous media is caused by the dissipation of viscous and kinematic energy, this energy loss is represented by a decrease in pressure. Ergun combined the theory of Reynolds and the method of Kozeny [21]. After numerous experiments, he corrected the parameters of the two relations which depend on the flow rates, namely, the linear relation with viscous energy loss and the term of $(1 - n_{\text{eff}})^2 / n_{\text{eff}}^3$, and the nonlinear relation with kinetic energy loss and the term of $1 - n_{\text{eff}} / n_{\text{eff}}^3$. So, by considering the effects of the particle size and shape, as well as extending the models from Kozeny–Carman in the linear laminar regime and the Burke and Plummer in the turbulent regime, the equation which he has proposed can generally describe all types of flow in the porous media. So, the Forchheimer coefficient for high flow rates can be expressed by the following equation:

$$\beta_E = \frac{1.75}{g} \cdot \frac{1 - n_{\text{eff}}}{n_{\text{eff}}^3} \cdot \frac{1}{D_p}, \quad (7)$$

where D_p is the particle diameter.

By combining the effects from the granular material with permeability, another approach to the Forchheimer coefficient can be expressed with the following equation:

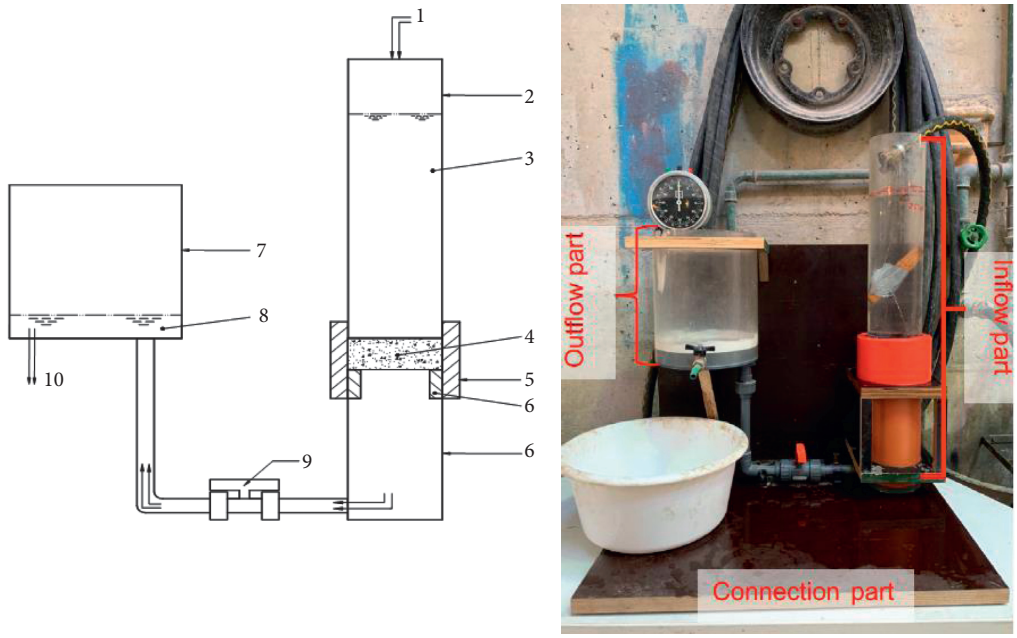

(a) (b)

FIGURE 4: Apparatus for permeability test. (a) Schematic diagram of apparatus (1: water inlet; 2: graduated plastic cylinder; 3: influent water head; 4: specimen; 5: upper rubber sleeve; 6: lower rubber sleeve; 7: outflow tube; 8: effluent water head; 9: water shut-off valve; and 10: water outflow). (b) Physical map of apparatus.

$$\mathscr{B}_w = \frac{0.55}{k^{0.5}}. \tag{8}$$

Based on the concept that considers the porous media as the capillaric model, many researchers contributed in this direction to theoretically analyze the flow behavior. Through the arrangement of these capillary tubes, these models can be distinguished into series and parallel bounded [19].

The equation for the parallel-type model can be expressed as follows:

$$\mathscr{B}_t^n = \frac{c_0}{K^{0.5} \cdot n_{eff}^{1.5}}. \tag{9}$$

And for the serial-type model,

$$\mathscr{B}_t^\tau = \frac{c_1 \cdot \tau}{K^{0.5} \cdot n_e}, \tag{10}$$

where $\mathscr{B}_t^n$ denotes the Forchheimer equation by applying the porosity, as well as $\mathscr{B}_t^\tau$ by using tortuosity, c_0 and c_1 are the constants, which denote the inertia and pore size distribution. From the previous study [13], the constants have been proposed for both models, which can properly estimate the flow behaviors in the clean-bed PUPM. So, the equations for the PUPM mixtures can be rewritten as the following equations:

The parallel-type model:

$$\mathscr{B}_t^n = \frac{0.0487}{K^{0.5} \cdot n_{eff}^{1.5}}. \tag{11}$$

The serial-type model:

$$\mathscr{B}_t^\tau = \frac{5.9435 \cdot 10^{-7} \cdot \tau}{k \cdot n_e}. \tag{12}$$

3. Results and Discussion

3.1. Clogging Concentration. During the clogging simulation, the clogging concentration in the first 30 minutes was observed. The influent, overflow, and effluent flow through the specimens during the clogging simulation were collected, and the clogging agents in the liquid were dried and weighed. The obtained data were analyzed and plotted in Figure 5. The results illustrate the increasing trends of clogging concentrations in both specimens. During the first 5 minutes of the clogging period, more than half of the clogging agents stuck in the PA 8, while these in the PUPM 8 were only 42%. The clogging concentration in PA 8 continued to rise sharply; after 20 minutes, the rate of growth became stable. After the loading time exceeded 30 minutes, more than 90% of the clogging agents can be found in PA 8. This denotes that the most hydraulic flow channels in PA 8 were blocked. By contrast, the clogging concentration in PUPM 8 increased slowly throughout the whole period. During the clogging periods, only around 52% of the clogging mass of the influent was accumulated in PUPM 8.

In conclusion, both specimens can be affected by the clogging issue. But the clogging situation in PUPM 8 is more optimal than that in PA 8.

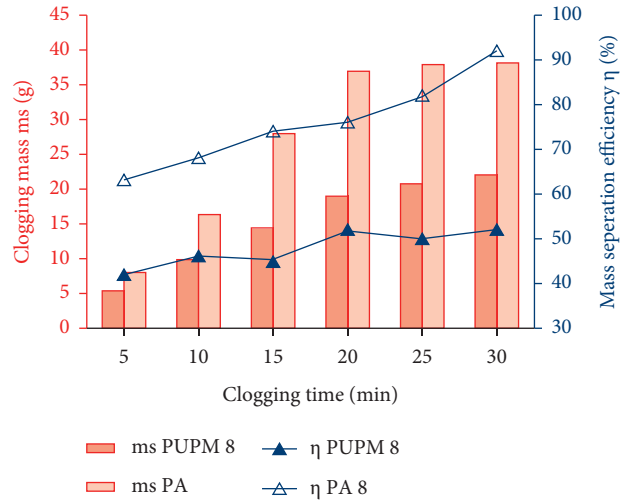

Figure 5: Plot of clogging concentrations in the PA 8 and PUPM 8 specimens during the clogging periods.

3.2. Permeability of Specimens during the Clogging Development. During the permeability test of the specimens, the data were collected in 5 hydraulic heads (from 100 to 300 mm with interval of 50 mm). In each level, four measurements for each specimen were recorded and then analyzed, respectively.

3.2.1. Flow Characteristics in terms of a Constant Hydraulic Head. As can be seen in Figure 6, the permeability coefficients at 300 mm hydraulic head of the specimens during the clogging periods were obtained. The specimens PUPM 8-H with the highest permeability can conduct 1.72×10^{-3} m/s of water. Followed by the PUPM 8 with the second highest permeability, and at the third position is the PA 8. In the figure, it can be recognized that the PUPM 8-L has the lowest permeability with 4.55×10^{-3} m/s.

For PA 8, the permeability of PA 8 decreased sharply once the clogging period started. In the first 20 minutes, the specimen's permeability sharply reduced from 1.08×10^{-3} m/s to 2.9×10^{-4} m/s, approximately 26% of its initial permeability. Conversely, during the same periods, the permeability of the PUPM 8 reduced slowly. Unlike the PA, the PU can perfectly cover the surface of the aggregates and provide a smooth surface for the aggregates. Therefore, the sediments can be easier caught in the PA specimen. The characteristic of the binder of the PA is, however, another influencing factor. Because of the high viscosity of the bitumen, the sediments tend to become attached to the bitumen. The flow behavior of the PA in the experiment is consistent with the previous study [13]. After 20 minutes of clogging simulation, the permeability of the PA 8 decreases continuously and steadily. 60 minutes later, the permeability of PA 8 reaches 7.5×10^{-5} m/s, which can be classified as permeable. However, the initial permeability was highly permeable. In comparison with the PUPM 8 and PUPM 8-H, the permeabilities of PA 8 are nineteen to thirteen times lower than that of PUPM 8 and PUPM 8-H.

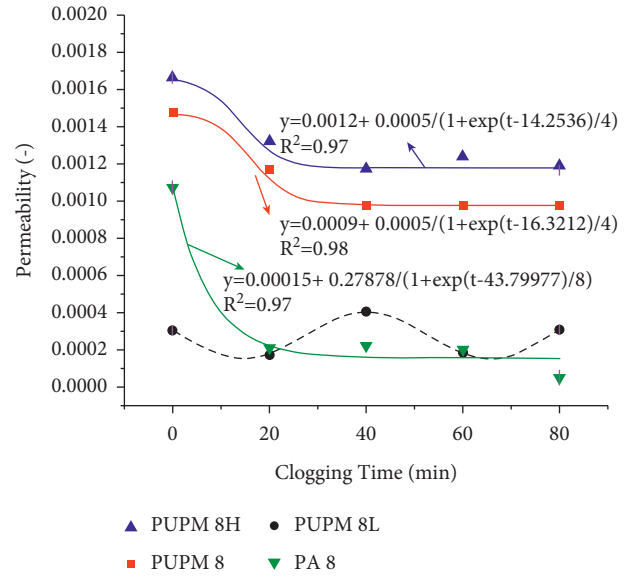

Figure 6: Plot of permeability coefficients for PUPM specimens and PA specimen at the hydraulic head of 300 mm during the clogging development [19].

With regard to PUPM 8, PUPM 8-H, and PUPM 8-L, according to Figure 6, two different decline trends of permeability coefficients can be observed. During the total clogging period, the permeability coefficients of the PUPM 8 and PUPM 8-H present similar downward trends. The permeability of the PUPM 8 reduced sharply, while this of the PUPM 8-H reduced much more steadily. After 80 minutes, the permeability of PUPM 8 reached 1.04×10^{-3} m/s, which is slightly lower than that of PUPM 8-H. By contrast, during the same clogging period, the permeability of PUPM 8-L shows a wave trend. A reason for this fluctuated trend could be that in the PUPM 8-L the continuous grading of aggregates was used, resulting in a high-density specimen with much lower porosity. In conjunction with that, the pressure from the tire of the clogging simulation and the impact of the flow causes two different effects. First, these forces push a little number of clogging agents into the specimen, while most of them stay on the surface of the specimen. Secondly, as the clogging loading time develops, some of these clogging agents would be then washed out by these forces. This consists of the shown permeability development of the PUPM 8-L. Nevertheless, after the whole clogging simulation, three kinds of PUPM can be classified as highly permeable.

In conclusion, all the four specimens have high initial permeability and can be affected by the clogging. However, the PA 8 is more influenced by the clogging than PUPM variants. After 80 minutes of clogging simulation, the permeability of all PUPM variants can still be recognized as highly permeable, but the PA 8 can be only classified as permeable.

3.2.2. Flow Characteristics in terms of Changing Hydraulic Gradients. This study is aimed to analyze the hydraulic properties of PUPM 8-H; the PUPM 8-L and PUPM 8 are no longer taken into consideration. By changing the hydraulic

head, the permeability coefficients of the specimens at the hydraulic gradient from 2.5 to 7.5 were evaluated and plotted in Figure 7. As can be seen from this figure, the rate of the permeability reduction slows down, as the clogging time and the hydraulic gradients increase. The study also found that the change of hydraulic gradient has a greater impact on the permeability coefficient without polishing, and this impact also decreases with the increase of polishing time.

As far as the flow behavior of the specimens, when the specimens were not subjected to the clogging, a non-Darcy flow behavior of all four specimens can be noticed. However, as the clogging time develops, the characteristic of linear flow become more obvious. It denotes that the viscous force is dominating the kinematic force, as the clogging development in the specimen. Nevertheless, as can be seen that at the clogging periods of 40 minutes, the permeabilities of the PUPM 8-H are the lowest during the whole clogging developments, which is not reasonable. Hence, an analysis for this can be conducted by combining with the pore characteristics of the specimens during the clogging development.

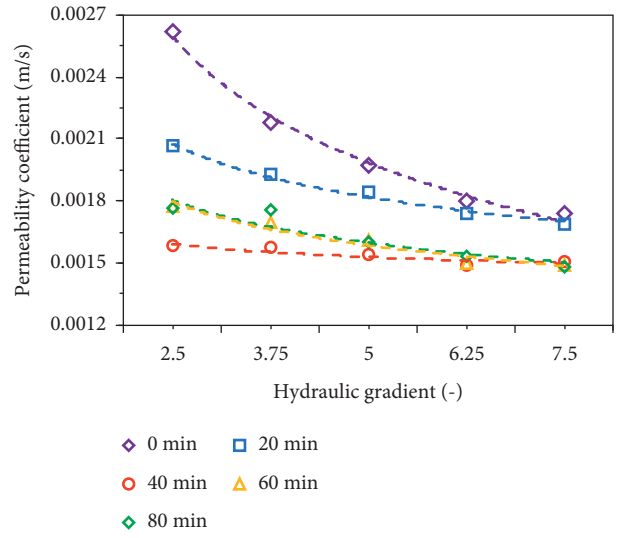

Figure 7: Plot of the variation of the permeability coefficients of PUPM 8-H at different hydraulic gradients during the clogging periods of 20, 40, 60, and 80 minutes.

3.3. Pore Characteristics during the Clogging. With the help of the XCT methods, the aid of MATLAB and Avizo software, the aggregate, polyurethane binder, and clogging mixture was successfully separated based on the OTSU method [13, 19]. The 3D visualization of PUPM 8-H is shown in Figure 8. The data of pore characteristics of the specimens during the clogging were thus obtained and analyzed.

The effective void content distribution, the specific surface area, and the tortuosity of the PUPM 8-H during the clogging periods are listed in Table 1. No obvious variant trends of PUPM 8-H during the whole clogging periods can be observed. However, combining the results of XCT analysis and the variation of the permeability by changing the applied hydraulic gradients, it can be noticed that with the increase of the value of tortuosity, the effective porosity of the specimens reduces faster. Additionally, the variation of its permeability during the clogging development follows the same trend. This denotes the fact that the tortuosity of the porous material affects its ability of resistance to the clogging particles. This could be the reason that the permeabilities at the clogging periods of 40 minutes are lower than those of other clogging periods, and the permeabilities at clogging periods of 80 minutes are similar with those at 60 minutes as well. To investigate the correlation of the pore characteristics that influence on the its permeability, it is assumed that a different tortuosity can be formed at a different clogging period; this would also cause a different clogging resistance, resulting in a different effective porosity; thus, a different permeability dissipation can be observed. To transfer this assumption into the mathematic equations, the initial porosity is multiplied by a clogging resistance term to obtain the effective porosity after a certain clogging period. This relationship can be expressed by the following equation:

$$n_{eff} = n_i \cdot c_R, \tag{13}$$

where n_{eff} is the effective porosity, n_i is the initial porosity of the PUPM 8-H, and c_R is the term of the clogging resistance. As assumpted that the tortuosity is a function of the clogging resistance term, the relationship between the clogging resistance and tortuosity was derived by fitting data, and it can be described by following equation:

$$c_R = 1.1958 \cdot e^{-0.469 \cdot \tau}, \tag{14}$$

where τ is tortuosity. By adopting equation (14) into (13), equation (13) can be rewritten as

$$n_{eff} = n_i \cdot 1.1958 \cdot e^{-0.469 \cdot \tau} \left(R^2 = 1\right). \tag{15}$$

Because the initial state of the specimen was not considered during the XCT scan analysis, the data of its pore characteristics are unknown. However, n_i of the PUPM 8-H can be approximated by fitting data and it has the value of 43.62.

3.4. Prediction of the Hydraulic Properties of PUPM during the Clogging Development. To estimate the hydraulic properties of the PUPM 8-H under the clogging effects, several models were carried out. From the flow velocity perspective, these properties were observed in two aspects.

3.4.1. Estimation of the Permeability of PUPM during the Clogging Development. As in the literature review mentioned, based on the pore characteristic parameters such as effective porosity, tortuosity, and specific surface area, the permeability of a porous material can be predicted with the KCM models. In this study, the results from XCT were modeled with three KCM models: the original KCM, the KCM GSD, and the modified KCM. The obtained permeability from these three models will be compared and discussed.

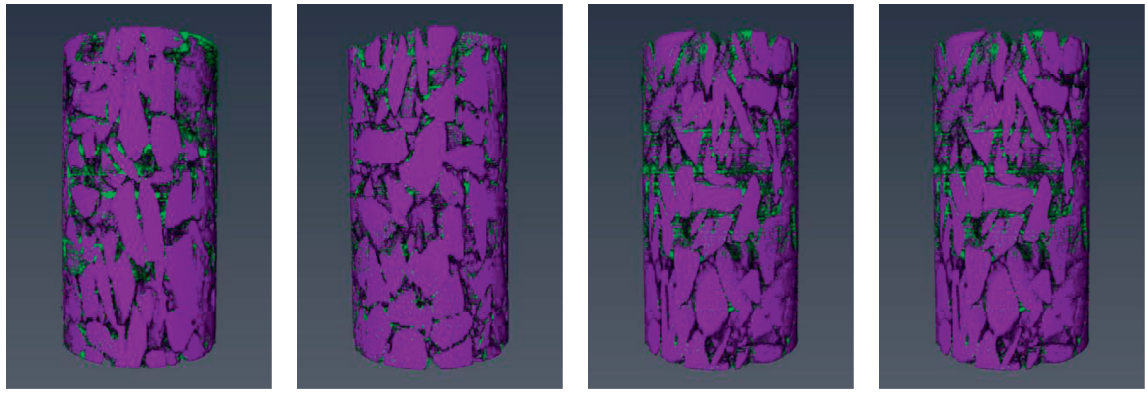

(a) (b) (c) (d)

Figure 8: 3D visualization of PUPM 8-H at the clogging period of (a) 20, (b) 40, (c) 60, and (d) 80 minutes [19].

Table 1: Void content distribution measurements for PUPM specimens at 20, 40, 60, and 80 min clogging simulation.

Specimens	Clogging time (min)	Effective void content (%)	Specific surface area ($1/m^{-1}$)	Tortuosity (-)
PUPM 8H	20	40.71	361.27	2.228
PUPM 8H	40	39.02	678.49	2.875
PUPM 8H	60	40.84	453.41	2.168
PUPM 8H	80	39.19	500.78	1.553

The permeability coefficients of PUPM 8-H, derived from three KCM models, were compared with the results of the measurement. The comparison is illustrated in Figure 9.

As expected, the original model has the highest dispersion from the measured permeability. As mentioned in the previous section, the focus of the original model was only on the porosity and the specific surface area of the materials, and all the aggregates are uniformly sharp. Thus, it delivers the most inaccurate results. The GSD model also delivered results with great deviations. In this model, the grain size distribution is taken into consideration. However, this parameter is highly dependent on uniform spheres and surrogate indices. The modified KCM has the best prediction for the permeability coefficients. In the modified KCM model, the tortuosity was taken into consideration because the aggregates of the material are irregular; through this, the pore structure in the porous material can be better described. This proves that the flow behavior can be modeled accurately only when the structure of the porous media is accurately described.

Compared with GSD and the original models, the modified model can predict the flow behavior in PUPM 8-H better, but it is not perfect. The modified KCM still cannot perfectly predict the flow behavior in the PUPM 8-H. The figure above shows that the values derived from this model are smaller than those measured in the permeability test. From the theoretical aspect, the modified KCM was used for the clean-bed specimens. Therefore, to predict the flow behavior of the porous media under the clogging periods accurately, the modified KCM model needs to be justified.

Based on the observation of the XCT results, the variation of the pore characteristics is very complicated. Regardless, a trend of the permeability coefficient of PUPM 8-H, which is similar to the exponential function, can be identified. The modified KCM model is incapable of estimating the permeability of the specimen perfectly. The deviation of the ascertained experimental data and the estimated permeability is caused by the clogging effect in the PUPM 8-H. To further improve the prediction on the permeability of the PUPM 8-H, the clogging issue is considered in a specific term, named the curve fitting function, and added to the modified KCM model in MATLAB. This curve fitting function was approximated to fit experimental data. Thus, the modified KCM in terms of the time-related clogging effects for the PUPM 8-H was derived. It is expressed as follows:

$$K^{c}_{\mathrm{KCM}} = \frac{\gamma_{\omega}}{\mu_{\omega} \cdot C_{k-c}} \cdot \frac{n_e}{\tau^2 S^2_{Ae}} \cdot \left(A_1 + A_2 * e^{\left(-A_3 * t\right)} \right), \quad (16)$$

where K^{c}_{KCM} is defined as the KCM permeability during the clogging periods. A_1, A_2, and A_3 are the coefficients. The values of these coefficients for equation (16) are listed in Table 2.

To test whether the modified KCM model for clogging can predict the permeability of the PUPM 8-H during the clogging periods properly, equation (16) was implemented for the calculation of the permeability of the PUPM 8-H. The results of both models were then compared with the measured permeability. These results are illustrated in Table 3.

As can be seen from the above table, the modified KCM model for clogging exhibits favorable results, as expected. In comparison with the modified KCM model and the modified KCM model for clogging, the relative error to the measured permeability coefficient is significantly lower for PUPM 8-H by applying the modified KCM model for clogging. Thus, in this case, it can be concluded, from comparing the maximum of the relative errors, that the estimated permeability can be more accurately calculated to be closer to the actual permeability in PUPM 8-H specimens during the clogging periods.

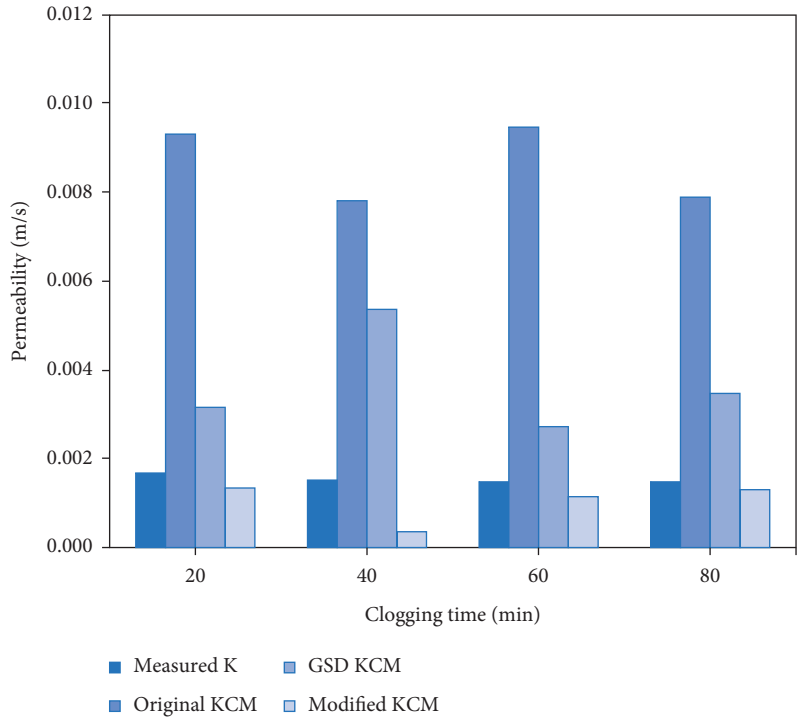

Figure 9: Comparison of measured permeability and estimated permeability with KCM models for PUPM 8-H during the clogging periods of 20, 40, 60, and 80 minutes.

Table 2: Constant parameters of the modified KCM models in terms of the clogging for PUPM 8-H.

Specimens	Constant parameters			
	A_1	A_2	A_3	R^2
PUPM 8-H	0.156	0.3	0.13	0.99

Table 3: Comparison results of permeability for PUPM 8-H.

Clogging time (min)	Measured K (m/s)	Modified KCM (m/s)	Relative error (%)	Modified KCM, clogging (m/s)	Relative error (%)
20	$1.69E-03$	$1.32E-03$	−21.86	$1.69E-03$	0.00
40	$1.50E-03$	$3.40E-04$	−77.31	$1.50E-03$	0.00
60	$1.48E-03$	$1.12E-03$	−24.02	$1.48E-03$	0.00
80	$1.48E-03$	$1.29E-03$	−12.90	$1.48E-03$	0.00

3.4.2. Estimation of the Non-Darcy Flow in the PUPM during Clogging Development. As stated in the previous section, the kinematic force in the porous material becomes significant, as the flow velocity increases. After a certain point, Darcy's law is no longer suitable to be applied to describe the flow behavior. To investigate the nonlinear flow behavior in the PUPM 8-H, the Reynolds number (Re) number and pressure drop were carried out.

Figure 10 shows the variation of values of the Re for the flows in the PUPM 8-H at the hydraulic gradients from 2.5 to 7.5 during the clogging development. According to Figure 10, growing trends of Re with the increase of the hydraulic gradients in the PUPM 8-H can be observed.

Many researchers suggest different values of the Re number to limit the upper threshold of Darcy's law; these values mostly range from 1 to 10. As can be seen from Figure 10, almost half of values of the Re for PUPM 8-H are found in the range of 1–10, which is a common phenomenon at a low hydraulic gradient. Therefore, the flow in PUPM 8-H is experiencing a critical region, where a transition period from the non-Darcy to the Darcy regime takes place.

In conclusion, within the applied hydraulic gradients, the values of Re for PUPM 8-H approach the Darcy regime area gradually with the increase of the clogging time. This is consistent with the conclusion from the permeability test in the previous section that the viscosity force in the specimens becomes notable with the increase of clogging development. Thus, Forchheimer's law is applicable for analyzing the behavior of non-Darcy flow in the PUPM 8-H.

Based on the existing study [13], the conventional Forchheimer models are needed to fit the prediction of the pressure drops in the PUPM 8-H to the actual measurements during the applied clogging periods. The nonlinear flow behavior in the PUPM 8-H can be predicted by fitting the capillaric models to the experimental data. To estimate this

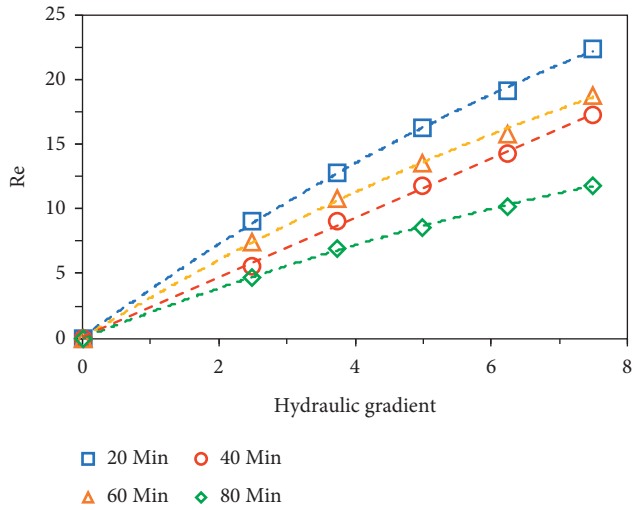

Figure 10: Plot of Re and hydraulic gradient for PUPM 8-H during the 20-, 40-, 60-, and 80-minute clogging periods.

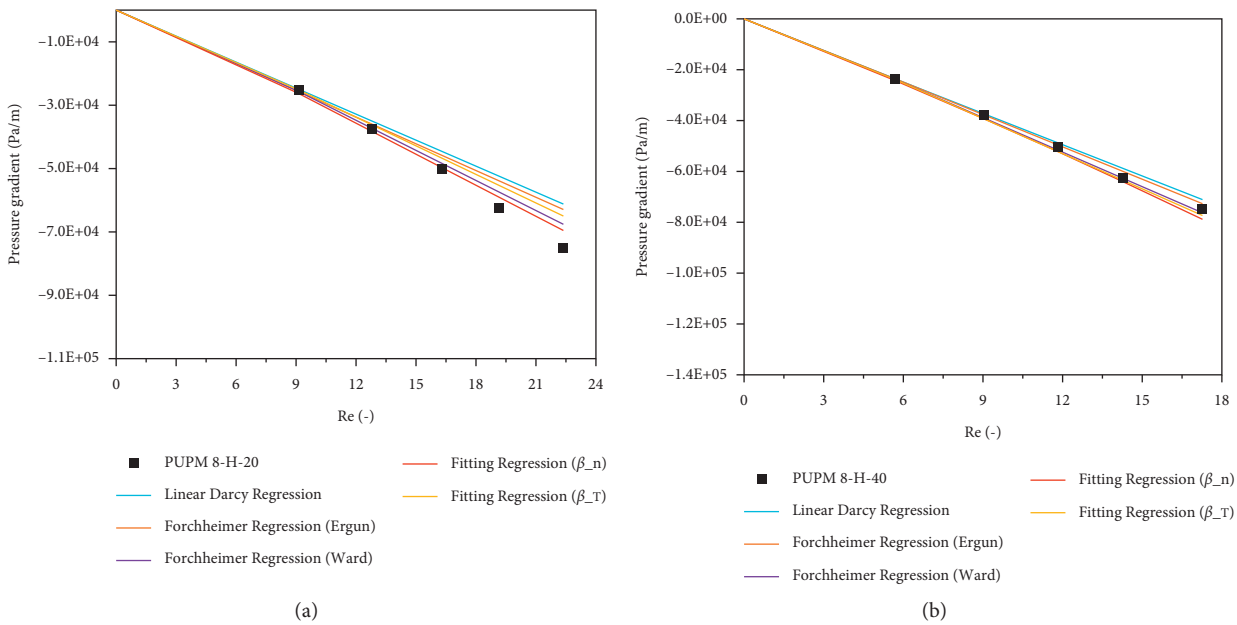

Figure 11: Continued.

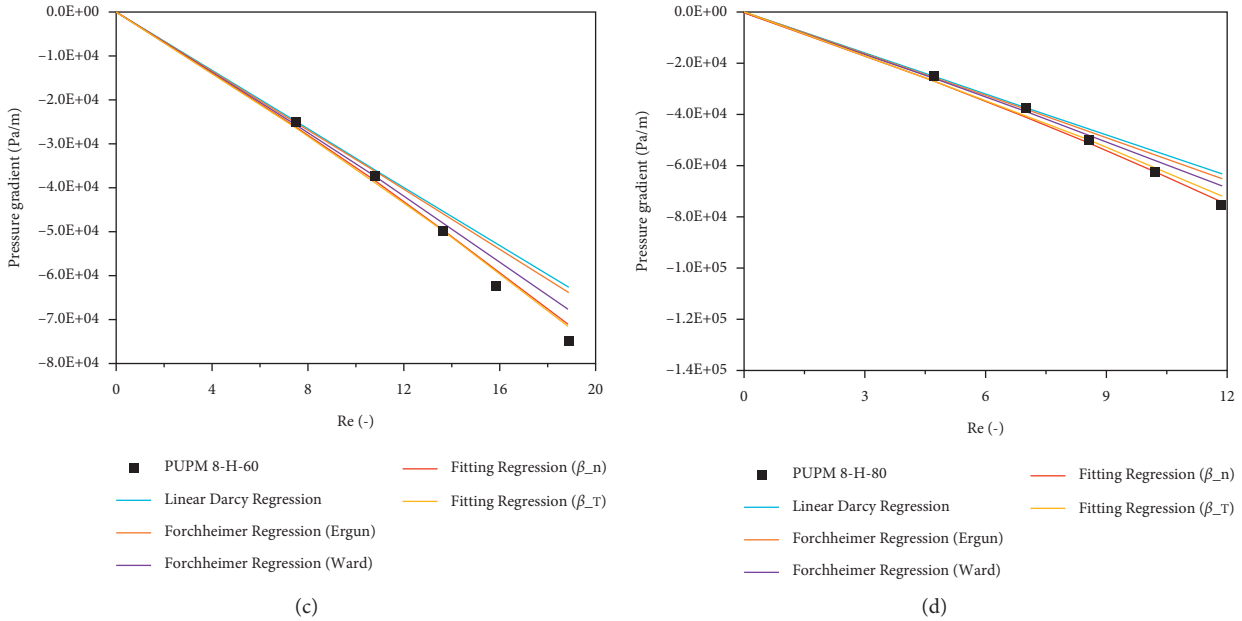

Figure 11: Modified Forchheimer's regressions and previous regressions for PUPM 8-H at different clogging periods (minutes): (a) 20; (b) 40; (c) 60; and (d) 80.

nonlinear flow behavior under the consideration of clogging, the curve fitting function in MATLAB was carried out.

For PUPM 8-H, the Forchheimer coefficient with the parallel type of the capillaric model can be remodeled as follows:

$$\mathscr{B}_c^n = \frac{0.0487 \cdot a_n \cdot e^{b_n \cdot t}}{k^{0.5} \cdot n_e^{1.5}}. \tag{17}$$

And with the serial type of the capillaric model,

$$\mathscr{B}_c^\tau = \frac{5.9435 \cdot 10^{-7} \cdot \left(a_\tau \cdot e^{b_\tau \cdot t} + c_\tau \cdot t\right) \cdot \tau}{k \cdot n_e}. \tag{18}$$

By adopting equations (17) and (18) into Forchheimer's law, the flow property of PUPM 8-H can be predicted as follows:

$$\nabla p_n^c = -\frac{\mu}{k_{\mathrm{KCM}}^m} v_D - \frac{0.0487 \cdot a_n \cdot e^{b_n \cdot t}}{k^{0.5} \cdot n_e^{1.5}} \rho v_D^2 \left(\mathrm{R}^2 = 0.97\right). \tag{19}$$

$$\nabla p_n^c = -\frac{\mu}{k_{\mathrm{KCM}}^m} v_D - \frac{5.9435 \cdot 10^{-7} \cdot \left(a_\tau \cdot e^{b_\tau \cdot t} + c_\tau \cdot t\right)}{k \cdot n_e} \tau \rho v_D^2 \left(\mathrm{R}^2 = 0.94\right), \tag{20}$$

where $a_{\mathrm{n}} = 2.6345$; $b_{\mathrm{n}} = 0.01035$; $\mathrm{a}_\tau = 0.2019$; $\mathrm{b}_\tau = 0.012$; and $\mathrm{c}_\tau = 0.0623$.

The predicted non-Darcy flow model can be seen in Figure 11.

As shown in Figure 11, during the whole clogging period, both remodified Forchheimer's equations gave closer results to the experimental measurements than those of Ergun and Ward's model. It can be concluded that the remodeled equations have a more accurate prediction for the nonlinear flow in the PUPM 8-H.

4. Conclusions

Based on the clogging simulation and permeability test, the clogging mechanism and development of hydraulic properties within the PPM were analyzed in depth. Detailed findings were listed in the following points:

(1) The initial permeability of the PUPM is higher than that of PA 8. During the clogging simulation with the Aachen Polishing Machine (APM), the permeability of PUPM decreases gradually, while in the PA 8, it

drops sharply in the first 20 minutes. After 80 minutes of the clogging simulation, the PUPM maintains a high permeability, while the PA 8 loses 74% of the initial permeability. It indicates that the PUPM can withstand the impact of the clogging agents with a size of up to 2 mm better than PA mixtures. Therefore, it can be concluded that the PUPM not only can provide a longer service lifespan but also has a significantly better water drainage performance than the PA mixtures.

(2) Based on the results from XCT, the pore characteristics such as the pore size, the porosity, the tortuosity, and specific surface area of the PUPM 8-H specimens were evaluated. Most values of all these characteristics during the clogging developments have no obvious trend. A relationship between the effective porosity and the tortuosity of the PUPM 8-H was found; it provides a clarification for the fluctuated trends of the pore characteristics.

(3) The equations related to the hydraulic properties of the PUPM 8-H in the clogging development were derived. They are based on the results from previous research and the clogging related term which was obtained from fitting the data of the permeability and pore characteristics of the PUPM 8-H. With the modeled equations, the loading time-dependent hydraulic conductivity and the pressure drops of the PUPM 8-H can be estimated [22].

Data Availability

The testing result data used to support the findings of this study are available from the corresponding author upon request.

Conflicts of Interest

The authors declare that they have no conflicts of interest regarding the publication of this paper.

Authors' Contributions

The authors confirm contribution to the paper as follows. Study conception and design: Pengfei Liu and Markus Oeser. Data collection: Guoyang Lu and Zhihao He. Analysis and interpretation of results: Guoyang Lu, Zijian He, Zhihao He, and Hao Jiang. Draft manuscript preparation: Guoyang Lu, Zijian He, Zhihao He, Pengfei Liu, and Gaoyang Li. All authors reviewed the results and approved the final version of the manuscript.

Acknowledgments

The work described in this paper was supported by a grant from the Germany/Hong Kong Joint Research Scheme sponsored by the Research Grants Council of Hong Kong (Ref. no. G-PolyU505/21) and the German Academic Exchange Service of Germany (Grant no. 57601840). The German Research Foundation (Grant no. OE 514/15-1, 459436571) is gratefully acknowledged as well.

References

[1] B. Huang, H. Wu, X. Shu, and E. G. Burdette, "Laboratory evaluation of permeability and strength of polymer-modified pervious concrete," *Construction and Building Materials*, vol. 24, no. 5, pp. 818–823, 2010.

[2] W. Sun, G. Lu, C. Ye et al., "The state of the art: application of green technology in sustainable pavement," *Advances in Materials Science and Engineering*, vol. 2018, 2018.

[3] N. Xie, M. Akin, and X. Shi, "Permeable concrete pavements: a review of environmental benefits and durability," *Journal of Cleaner Production*, vol. 210, pp. 1605–1621, 2019.

[4] Z. Teng and J. Sansalone, "In situ partial exfiltration of rainfall runoff. II: particle separation," *Journal of Environmental Engineering*, vol. 130, no. 9, pp. 1008–1020, 2004.

[5] S.-S. Pathapati and J. J. Sansalone, "Modeling particulate matter resuspension and washout from urban drainage hydrodynamic separators," *Journal of Environmental Engineering*, vol. 138, no. 1, pp. 90–100, 2012.

[6] W. D. Carrier, "Goodbye, hazen; hello, kozeny-carman," *Journal of Geotechnical and Geoenvironmental Engineering*, vol. 129, no. 11, pp. 1054–1056, 2003.

[7] S. Ergun, "Fluid flow through packed columns," *Chemical Engineering Progress*, vol. 48, pp. 89–94, 1952.

[8] D. Li and T. W. Engler, "Literature review on correlations of the non-Darcy coefficient," in *Proceedings of the SPE Permian Basin Oil and Gas Recovery Conference*, OnePetro, Midland, Tex, USA, May 2001.

[9] J. Zhang, F. Li, L. Zeng, J. Peng, and J. Li, "Numerical simulation of the moisture migration of unsaturated clay embankments in southern China considering stress state," *Bulletin of Engineering Geology and the Environment*, vol. 80, no. 1, pp. 11–24, 2021.

[10] J. Zhang, R. She, Z. Dai et al., "Experimental simulation study on pore clogging mechanism of porous pavement," *Construction and Building Materials*, vol. 187, pp. 803–818, 2018.

[11] H. Zhou, H. Li, A. Abdelhady, X. Liang, H. Wang, and B. Yang, "Experimental investigation on the effect of pore characteristics on clogging risk of pervious concrete based on CT scanning," *Construction and Building Materials*, vol. 212, pp. 130–139, 2019.

[12] J. Zhang, X. Cui, L. Li, and D. Huang, "Sediment transport and pore clogging of a porous pavement under surface runoff," *Road Materials and Pavement Design*, vol. 18, no. sup3, pp. 240–248, 2017.

[13] J. Jiang, Z. Zhang, Q. Dong, and F. Ni, "Characterization and identification of asphalt mixtures based on convolutional neural network methods using X-ray scanning images," *Construction and Building Materials*, vol. 174, pp. 72–80, 2018.

[14] G. Lu, Z. Wang, P. Liu, D. Wang, and M. Oeser, "Investigation of the hydraulic properties of pervious pavement mixtures: characterization of Darcy and non-Darcy flow based on pore microstructures," *Journal of Transportation Engineering, Part B: Pavements*, vol. 146, no. 2, Article ID 04020012, 2020.

[15] G. Lu, P. Liu, T. Törzs, D. Wang, M. Oeser, and J. Grabe, "Numerical analysis for the influence of saturation on the base course of permeable pavement with a novel polyurethane binder," *Construction and Building Materials*, vol. 240, Article ID 117930, 2020.

[16] G. Lu, L. Renken, T. Li, D. Wang, H. Li, and M. Oeser, "Experimental study on the polyurethane-bound pervious mixtures in the application of permeable pavements," *Construction and Building Materials*, vol. 202, pp. 838–850, 2019.

[17] G. Lu, T. Törzs, P. Liu et al., "Dynamic response of fully permeable pavements: development of pore pressures under different modes of loading," *Journal of Materials in Civil Engineering*, vol. 32, no. 7, Article ID 04020160, 2020.

[18] G. Lu, H. Wang, T. Törzs et al., "In-situ and numerical investigation on the dynamic response of unbounded granular material in permeable pavement," *Transportation Geotechnics*, vol. 25, Article ID 100396, 2020.

[19] S. Xu, G. Lu, B. Hong et al., "Experimental investigation on the development of pore clogging in novel porous pavement based on polyurethane," *Construction and Building Materials*, vol. 258, Article ID 120378, 2020.

[20] G. Lu, P. Liu, Y. Wang, S. Faßbender, D. Wang, and M. Oeser, "Development of a sustainable pervious pavement material using recycled ceramic aggregate and bio-based polyurethane binder," *Journal of Cleaner Production*, vol. 220, pp. 1052–1060, 2019.

[21] X. Kuang, J. Sansalone, G. Ying, and V. Ranieri, "Pore-structure models of hydraulic conductivity for permeable pavement," *Journal of Hydrology*, vol. 399, no. 3-4, pp. 148–157, 2011.

[22] J. Zhang, J. Peng, L. Zeng, J. Li, and F. Li, "Rapid estimation of resilient modulus of subgrade soils using performance-related soil properties," *International Journal of Pavement Engineering*, vol. 22, no. 6, pp. 732–739, 2021.